

Shear-Induced Cyclo-Reversion Leading to Shear-Thinning and Autonomous Self-Healing in an Injectable, Shape-Holding Collagen Hydrogel

*Mahsa Jamadi Khiabani¹, Sareh Soroushzadeh², Ardeshir Talebi², and Ayan Samanta*¹*

¹Macromolecular Chemistry, Department of Chemistry – Ångström Laboratory, Uppsala University, Box 538, 751 21 Uppsala, Sweden

²Department of Pathology, School of Medicine, Isfahan University of Medical Sciences, Isfahan, Iran

KEYWORDS. Click Chemistry, Bio-Orthogonal Reaction, Collagen Hydrogel, Furan-Maleimide Diels-Alder Reaction, Shear-Thinning, Autonomous Self-Healing, Cardiac Tissue Engineering, Cyclo-Reversion, Mechanophore, Shape-Holding, Injectable.

ABSTRACT

In vivo injectable extracellular matrix (ECM) derived hydrogel that is suitable for cell encapsulation has always been the holy grail in tissue engineering. Nevertheless, these hydrogels still fall short today of meeting three crucial criteria: flexibility on the injectability time-window, autonomous self-healing of the injected hydrogel, and shape-retention under aqueous conditions.

Here we report the development of a collagen-based injectable hydrogel, crosslinked by cycloaddition reaction between furan and maleimide groups, that is injectable up to 48 hours after preparation and can undergo complete autonomous self-healing after injection. Furthermore, this hydrogel can retain its shape and size over several years when stored in buffer, yet can be degraded within hours when treated with collagenase. The biocompatibility of this hydrogel was demonstrated *in vitro* by cell-culture and *in vivo* by subcutaneous implantation in rats.

INTRODUCTION

In recent years injectable hydrogels have gained enormous interest in the field of biomaterials as they can be administered through a minimally invasive surgery and can fill in defects of any size and shape.¹ However, *in vivo* injectability through a 27-gauge needle and quick setting of the hydrogel at the injection site would require the hydrogel precursor solutions to have low enough viscosity to allow passing through the narrow needle smoothly and yet form a hydrogel almost immediately to prevent dissolution of the hydrogel and burst release of the encapsulated cells or drugs. Moreover, the injected hydrogel should be degradable in the host to avoid causing foreign body response which can lead to fibrosis.² Additionally, if the injectable hydrogel is to be used for cell-delivery, the gelation should be slow enough to allow proper mixing and even distribution of cells within the matrix but fast enough to prevent agglomeration and sedimentation of the cells.³ Extensive efforts are thus often dedicated to fine-tuning the gelation time by varying the number of cross-linkable groups in the polymer chain, altering total polymer concentration in the hydrogel, varying catalyst concentration or by using external or *in vivo* stimuli.⁴ Moreover, it is desirable that the hydrogel is shear-thinning to protect the encapsulated cells from the shear-stress exerted upon during the injection and autonomously self-healing to restore the hydrogel mechanical properties resulting in a cohesive uniform hydrogel after injection. Encouraged by this idea, several

shear-thinning and self-healing hydrogels were developed.⁵ Despite substantial developments to date, injectable hydrogels suffer from a major drawback; they swell and cannot hold their shape.⁶ Unwanted swelling exerts pressure on the surrounding tissues resulting in edema-like conditions. Moreover, in most cases the self-healing of the injected hydrogel requires an external trigger. Hence, there is an unmet need for injectable, shear-thinning, and autonomous self-healing hydrogels which hold their shape, do not swell, and is degradable in the host.

Hydrogels made from collagen, the most abundant component in extracellular matrix (ECM), demonstrated to promote regeneration of various tissues and can be easily remodeled *in vivo*. Moreover, collagen bears focal-adhesion sites for cells, and therefore, collagen hydrogels do not require additional functionalization with bioactive peptides for cell spreading and proliferation. While collagen can self-assemble, a process known as fibrillation, at physiological pH, temperature, and salt concentration to form a hydrogel, such physically assembled collagen hydrogels are too soft for surgical manipulations, and results in excessive swelling, too quick dissolution, and is prone to rapid enzymatic degradation.⁷ One potential solution to this problem would be to chemically crosslink the collagen molecules to form a hydrogel since permanent covalent bonds are more stable than physical interactions and should prevent excessive swelling and too rapid dissolution *in vivo*. Hence, we and others have developed chemically crosslinked collagen hydrogels employing the pendant amines and carboxylic acids from the side-chains of collagen.⁸⁻¹⁴ However, such crosslinking chemistries developed to date are toxic. If such hydrogels need to be injected *in vivo*, the crosslinking reaction needs to be quenched prior to injection.^{15, 16} This defeats the purpose of chemical crosslinking as often incomplete crosslinking leads to a very soft hydrogel. Alternatively, injection of the hydrogel after complete crosslinking results in a non-

cohesive crushed gel. In either case, cell-delivery using such hydrogels is highly challenging due to the toxic nature of the crosslinking chemistry.

Therefore, researchers have adopted a strategy where the collagen is modified with functional groups other than amines or carboxylic acids to be able to use less or non-toxic crosslinking reactions. A popular strategy relies on photo-initiated radical polymerization. Consequently, several modified collagen hydrogel systems were developed that requires UV or visible light for radical-mediated crosslinking.¹⁷⁻²⁰ However, limited penetration depth of UV or visible light and generation of free-radicals are noticeable drawbacks of these hydrogels.²¹ As a result, alternative systems that do not involve free-radicals and rely on light will be valuable.

Recently, we have developed bio-orthogonally crosslinked injectable, shear-thinning, and shape-holding collagen hydrogels employing Michael addition reactions involving thiols and Michael acceptors such as maleimide or (meth)acryloyl functional groups.²²⁻²⁴ Some of them are partly self-healing due to the slow crosslinking and reversibility of the reaction in presence of excess thiols.^{22, 24} Nonetheless, a major drawback of hydrogel systems relying on thiols is the lack of control on side reactions involving thiols, especially oxidation of thiols to disulfides, which renders the storage of thiol collagen challenging. Furthermore, a complete and autonomous self-healing of the hydrogels after injection was not achieved.

The most promising approach to address the instability issue of thiol-collagen is to introduce collagen modifications that will undergo bio-orthogonal cycloaddition reactions without requiring light since majority of the dienes and dienophiles are more stable than thiols. Furthermore, fast reaction rates and absence of by-product formation classify them as “click” reactions. In the past years, several examples include the use of cycloaddition reactions for the preparation of bio- and nanomaterials.²⁵ Strain-promoted azide alkyne cycloaddition (SPAAC) is

of particular interest as injectable collagen hydrogel crosslinked using SPAAC has been developed for *in situ* filling of corneal defects and demonstrated to support the regeneration of corneal epithelium *in vivo*.^{26, 27} However, these hydrogels are injectable only during the early phase of gelation and not self-healing. This is attributed to the irreversible nature of SPAAC. Among other cycloadditions, the reaction between norbornene and tetrazine has been employed to prepare hydrogels from ECM-derived polymers.^{28, 29} Similarly, these hydrogels were not injectable owing to the very fast and irreversible nature of the crosslinking reaction.

A notable example among cycloadditions is the reaction between furan and maleimide. Furan-maleimide cycloaddition reaction has been successfully employed earlier to develop cell-laden hydrogels,³⁰⁻³⁴ hydrogels emulating the ECM,³⁵ tough hydrogels,³⁶ stimulus dependent self-healing hydrogels,³⁷ and for sustained delivery of drugs or therapeutic factors.^{38, 39} Furthermore, furan maleimide cycloaddition reaction has been recently used for preparing gelatin-based hydrogels,^{40, 41} drug delivery,⁴² and for developing nanoparticle carrying hydrogels.⁴³⁻⁴⁶ However, temperature as high temperature as 65 °C was needed to perform the crosslinking leading to hydrogel formation. Furthermore, these hydrogels were non-injectable and lacked self-healing properties at ambient temperature, and in some cases required incubation at 37 °C for 5 hours to achieve self-healing following a single incision.³⁷

To date no example of injectable collagen hydrogel exists which could undergo autonomous self-healing after injection. Although, we have developed several bio-orthogonally crosslinked injectable, shear-thinning collagen hydrogels with shape-retaining property, autonomous self-healing could not be achieved. Here we report an injectable collagen hydrogel crosslinked through the cycloaddition reaction between furan and maleimide which undergoes complete autonomous self-healing at ambient temperature after injection. The developed hydrogel

is shear-thinning and can be injected in gel state up to after 2 days of preparation. Furthermore, this hydrogel can hold its shape after prolonged storage in buffer and yet can be degraded within hours *in vitro* by collagenase and can be resorbed completely within two months *in vivo*. Last but not the least, cardiac stem cells and endothelial cells can be encapsulated in these hydrogels without any noticeable toxicity.

RESULTS

Synthesis and characterization of collagen furan. Furan group was installed onto collagen through functionalization of the pendant amines from lysine and arginine side chains by reaction with furfuryl glycidyl ether (**Figure 1A**). The pKa of these amines is 10.5 and therefore, the reaction was performed at pH 10 to ensure the deprotonated state of the amine for a nucleophilic ring opening reaction. Protein modification through pendant amines by reacting with glycidyl moieties is well-established. The resulting collagen furan (CF) was analyzed by ¹H NMR spectroscopy and the appearance of peaks at 6.38, 6.41 and 7.46 δ ppm was attributed to the aromatic protons of the furan group (**Figure 1D**). The degree of modification was determined by TNBS colorimetric assay and was found to be 61.4%±1.8% with respect to the amines in collagen. Moreover, circular dichroism spectroscopy was employed to ensure the structural integrity of the polyproline II triple helix in collagen furan. Both pristine collagen and collagen furan showed a negative ellipticity peak at 190 nm and a positive ellipticity peak at 220 nm which are characteristic of polyproline II triple helix (**Figure S1**).⁴⁷ This data confirm the preservation of collagen triple helix in collagen furan.

Collagen is well-known for lower critical solution temperature (LCST)-like transition and gel formation where the viscosity of collagen solution increases if the temperature is raised from 25 to 37 °C. This LCST-like transition is also responsible for collagen fibrillation at physiological

pH and temperature. Temperatures higher than normal physiological temperature, however, causes melting of the collagen fibrillar assembly. Hence, a 2 w% collagen furan solution has also been assessed for its capability of similar gel formation by oscillatory rheology where the complex viscosity (η^*) was measured over a temperature range from 25 to 50 °C and compared with 2 w% pristine collagen solution. Both pristine collagen and collagen furan showed a slight increase in η^* by increasing the temperature from 25 °C and attained the highest value at 28 °C for pristine collagen and 36 °C for collagen furan, indicating fibrillation (**Figure 1E**). Further increase in temperature resulted in decrease of complex viscosity which reached a stable value at 45 °C for both pristine collagen and collagen furan. Moreover, the loss tangent ($\tan \delta$) increased with increasing temperature indicating more damping and energy dissipation in the gel as can be expected due to the increased mobility of the individual collagen molecules within the intermolecular assembly at higher temperature. The loss tangent reached its maxima at 39 and 45 °C for pristine collagen and collagen furan, respectively, indicative of the melting of the collagen triple helix at these temperatures.^{48,49} A higher triple helix melting temperature could be attributed to the stabilization of the triple helix rendered by the hydrophobic furan modifications in collagen furan. It was demonstrated earlier for collagen mimetic peptides that hydrophobic modifications bestow hyperstability in polyproline II triple helix.⁵⁰ Moreover, above the melting temperature of the polyproline II triple helix, pristine collagen solution behaved as a viscous liquid with a $\tan \delta$ higher than unity whereas collagen furan still demonstrated a gel-like behavior with $\tan \delta$ value residing below unity (**Figure 1E**). To our understanding, this is due to the hydrophobic associations between the furan groups on the random coil of collagen polypeptide after melting of the polyproline II triple helix.

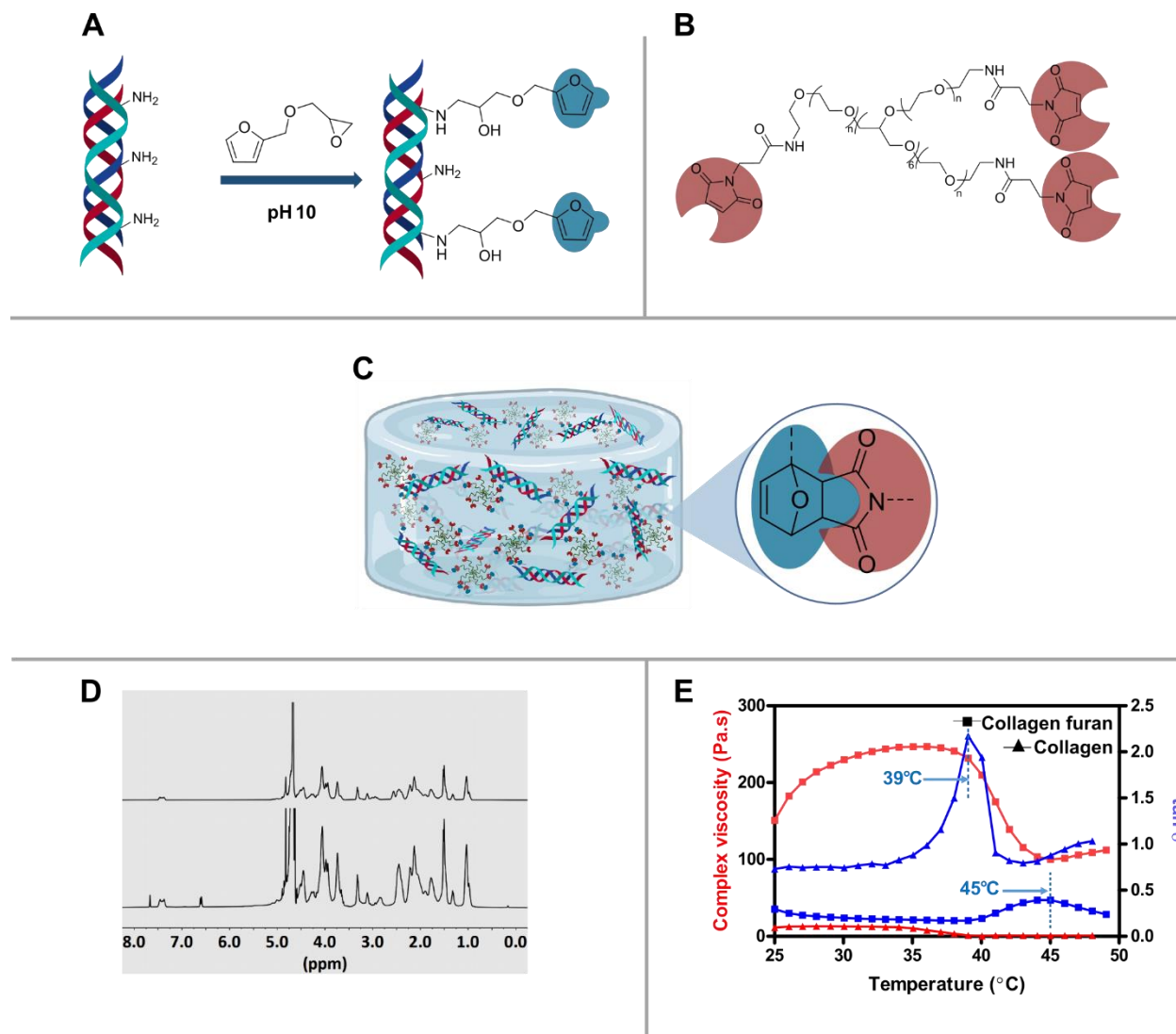


Figure 1. Overview of the collagen furan hydrogel. **A.** Reaction scheme for the synthesis of collagen furan. **B.** Chemical structure of the 8-arm polyethylene glycol maleimide (PEG-maleimide). **C.** Schematic of collagen furan - PEG maleimide hydrogel with chemical structure of the cycloaddition product. **D.** ^1H NMR spectra in D_2O of pristine collagen (top) and collagen furan (bottom). **E.** Effect of temperature on the viscoelastic behaviors of 2% (w/v) collagen and collagen furan aqueous solutions.

Preparation of hydrogel. To demonstrate the formation of chemically crosslinked hydrogel via cycloaddition between furan and maleimide groups, solutions of collagen furan and 8-arm PEG-maleimide in PBS were mixed together at pH 5-6. Crosslinking was qualitatively confirmed by lifting the hydrogel from the mold with a tweezer or spatula.

Furthermore, the time required for complete gelation was examined at 25 and 37 °C. For this purpose, the precursors of **r2** hydrogel (**Supplementary Table 1**) were mixed together, cast onto the rheometer plate, and the storage and loss moduli were monitored over 44 hours (**Figure S2**). As non-crosslinked collagen solution is known to behave as a gel ($G' > G''$) above 0.5% concentration at 1Hz,⁴⁹ a typical sol-gel transition was not possible to observe for collagen furan hydrogel formation. Rather the gradual increase of storage modulus over time was considered as gelling due to covalent crosslinking, and the time required to obtain a plateau in storage modulus was considered as the time needed for complete gelation. Nonetheless, storage modulus of our developed hydrogel did not reach a plateau over 44 hours (**Figure S2**). The rate of increase of storage modulus was slightly higher at 37 °C compared to 25 °C (**Figure S2**) as expected since the reaction can proceed faster at a higher temperature and collagen undergoes fibrillation leading to gel formation at 37 °C. Hence, **r2** hydrogels were prepared separately and kept in the mold for different duration (1, 3, and 7 days) before subjecting them to rheological amplitude sweep for determination of storage and loss moduli. As shown in **Figure 2A**, storage modulus increased significantly with changing the curing time from one day to three days. In contrast, from day 3 to day 7, there was not a significant increase in the storage modulus.

Viscoelastic properties of collagen furan hydrogel. In an earlier study with chemically crosslinked injectable collagen hydrogel, we demonstrated that hydrogel moduli can be very easily fine-tuned by controlling the number of covalent crosslinks formed through varying the

stoichiometry between reaction partners.²⁴ Although this is trivial for hydrogels prepared using synthetic polymer, such as polyethylene glycol, with low molecular weights where covalent crosslinks are the sole determinants of elasticity,⁵¹ this is not the case for ECM-polymer based hydrogels where elasticity also originates from the self-assembly of polymer chains as well as chain entanglements. Earlier studies involving native telopeptide-rich collagen and matured telopeptide-poor collagen revealed more chain entanglements in case of telopeptide-rich collagen.⁵² Since the collagen used in our studies is telopeptide-poor, it is rational to assume that there will not be much chain entanglements in the crosslinked hydrogels from collagen or from the PEG since the molecular weight of the PEG is low.⁵³ However, the collagen will tend to assemble leading to elastic contribution and it could be impossible to fine-tune the collagen hydrogel moduli by only varying the covalent crosslinks. This was found to be true in one of our earlier studies.²² However, in an effort to fine-tune the hydrogel moduli, different stoichiometric ratios of furan to maleimide were investigated using oscillatory rheology (**Figure S3**). With increasing the furan to maleimide ratio from 1 to 2, the G' (3245 ± 218 Pa vs 4010 ± 165 Pa) and G'' (380 ± 23 Pa vs 463 ± 37 Pa) increased further ($p < 0.05$); however, further increasing of maleimide to furan ratio has no significant effect on G' and G'' values, (**Figure S3 B and C**). The loss tangents were found to have no statistically significant differences among various formulations (**Figure S3 D**).

Compression properties of collagen furan hydrogels. To test the mechanical properties of the collagen-furan hydrogels, unconfined compression was performed on different hydrogel formulations with varying furan to maleimide ratios (**r1-r4**) (**Figure S4**). The **r2** hydrogel demonstrated to have a compressive modulus of 7.42 ± 0.94 kPa which was found to be significantly higher than **r1** hydrogel (**Figure S4 A**). However, no statistically significant

differences could be observed for compressive strength and strain among all formulations (**Figure S4 B & C**). All following experiments were performed using **r2** hydrogel.

Injectability and shear-thinning properties of collagen furan hydrogel. To evaluate the injectability and shear-thinning properties of hydrogels, all components of **r2** hydrogel were mixed in the syringe mixing system, and the crosslinking reaction was allowed to proceed in the syringe for different period of time (0h, 4h, and 48h), followed by extrusion through a 27 G needle from the syringe onto the rheometer plate. Afterward, viscosity under continuous shear was measured with increasing the shear rate from 0.01 to 100 s⁻¹ as shown in **Figure 2B**.

In an earlier study involving synthetic polymer network for the preparation of elastomers and thermosets, the furan-maleimide cycloadduct was reported to undergo cyclo-reversion at high temperature.⁵⁴ To our understanding, the shear force generated during injection at 25 °C acts as a force-actuator mimicking elevated temperature resulting in mechanochemical decoupling of the cycloadduct.⁵⁵⁻⁵⁸ Furthermore, these hydrogels were injectable at least up to 48 hours after mixing of the precursors when stored at room temperature (**Figure 2B, 2C**).

Enzymatic degradation and swelling of hydrogel. To evaluate enzymatic degradation, hydrogels were incubated in collagenase solution *in vitro*; as a result, the hydrogels were degraded to a degree that made it impossible to weigh them after 6 h and completely dissociated soon after (**Figure 2D**).

For clinical applications, where the gel is injected to the tissue defect in order to fill the cavity, it is important that the injected hydrogel does not swell too much as prolonged swelling will cause enhanced pressure on the tissue around the injection site and risk the hydrogel popping out of the defect. On the other hand, poor mechanical strength after swelling has always been a major disadvantage of injectable hydrogels. In this study, the swelling ratio (wet/wet swelling ratio) was measured by evaluating the equilibrium hydrogel weight after 24 hours of swelling in

PBS at 37 °C to as prepared weight determined immediately after crosslinking to understand how much collagen furan hydrogel might swell after injection and crosslinking. As shown in **Figure 2E**, the collagen furan hydrogel showed minor swelling degree of 10 % after 24 hours from the as prepared state. This small extent of swelling was not visible in observations through naked eye (**Figure 2F**). As minor swelling was observed, a swelling experiment over 5 days was performed in a similar manner which revealed no significant swelling when compared to 24 hours of swelling (**Figure 2E inset**). By introducing hydrophobic furan to the collagen polymer chain and further crosslinking with maleimide group, the overall hydrophilicity of the polymer network decreases with concomitant increase in elasticity of the network, leading to lower swelling.

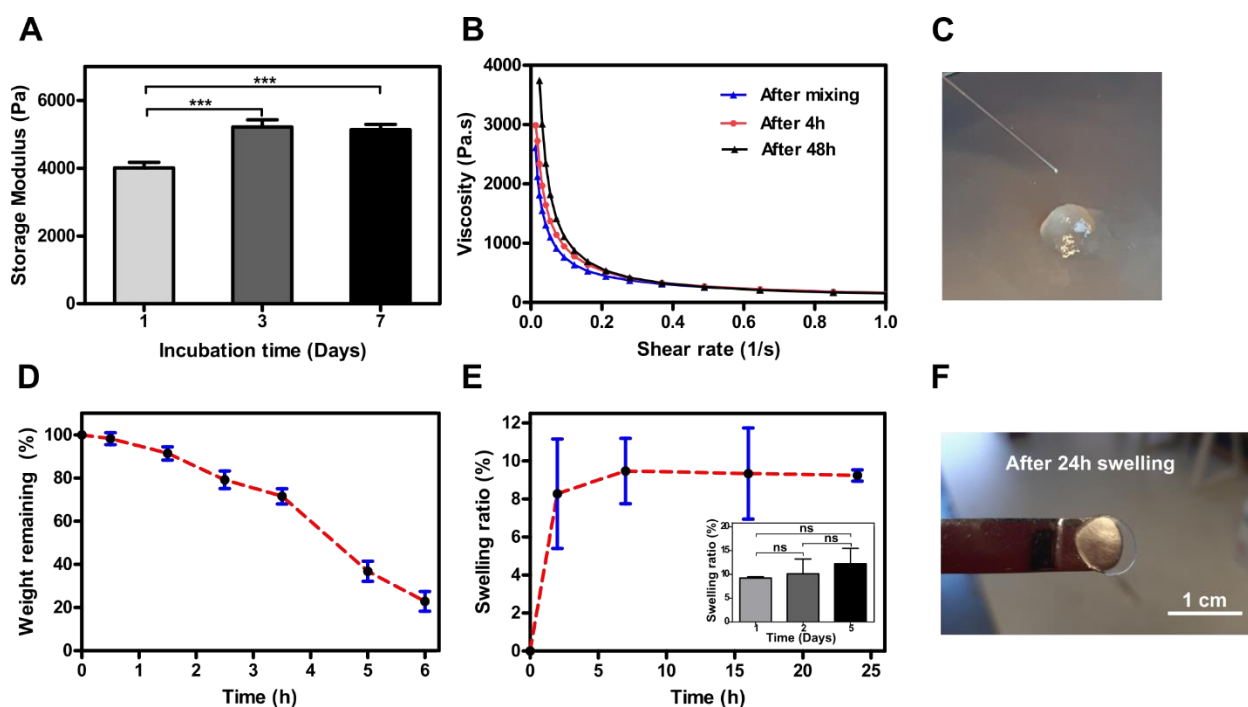


Figure 2. Assessment of gelation, shear-thinning, enzymatic degradation, and swelling properties of collagen furan hydrogels. **A.** The storage moduli at 1 % strain and 1 Hz oscillation frequency of **r2** hydrogel samples were compared at various time points to find out the time required for complete gelling ($F_{42,25}$, df_6). **B.** Injectability and shear-thinning properties of collagen furan

hydrogels; viscosity at increasing shear rate measured at immediately, 4h, and 48h after hydrogel preparation. **C.** Photograph of the injection experiment 48h after hydrogel preparation from a 27 G needle. **D.** Enzymatic degradation of collagen furan hydrogels in collagenase solution (5 U/mL), expressed as a percentage of initial weight remaining. **E.** Swelling of collagen furan hydrogels stored in PBS at 37 °C for 24h; inset: swelling over 5 Days. **F.** Photograph of collagen furan hydrogel after 24h swelling (with the original shape of 8-mm diameter disc), scalebar = 1 cm. All experiments were performed with **r2** hydrogels (**Table S1**). Error bars represent standard deviation, "****" represents a p-value of ≤ 0.001 ; df represents degrees of freedom; one-way ANOVA, followed by Tukey's test, n = 3 independent samples.

Autonomous self-healing after extrusion. To evaluate the self-healing of the developed hydrogels after extrusion, all components were mixed together and kept in the syringe mixing system for 48 h at room temperature (r.t) for the crosslinking reaction to proceed. Afterwards, the formed hydrogel was extruded (**Figure 3A**) onto a glass slide and incubated in the mold for 24 h at r.t (**Figure 3B**). Then, the hydrogel was demolded and incubated in PBS for 3 days at r.t (**Figure 3B**) followed by rheology amplitude-sweep to determine the modulus and linear viscoelastic region of the reformed hydrogel (**Figure 3 C-E**). In a parallel experiment the extruded hydrogel as described in **Figure 3A** was subjected to rheology time-sweep for the assessment of rate of re-gelation (**Figure 3F**). The extruded hydrogels were reformed without needing any external trigger resulting in a homogeneous hydrogel that could be picked up by a spatula (**Figure 3C**). To further quantitatively assess the self-healing of the extruded hydrogels, oscillatory amplitude sweeps were performed and compared side-by-side with original hydrogels (**Figure 3 D, E**). To our surprise, no statistically significant differences could be observed between original and reformed samples in terms of storage and loss moduli (**Figure 3E**) and the graph of G' vs oscillation strain was found

to be nearly identical for both original and reformed hydrogels (**Figure 3D**). This had led us to conclude that the self-healing is quantitative in terms of stiffness, indicated by G' , and linear viscoelastic region, indicated by the G' vs oscillation strain graph. Moreover, time-sweep rheology revealed that the rate of re-gelation of the extruded hydrogels were nearly identical to that of the original hydrogel (**Figure 3F**). To our understanding, the shear force during extrusion acted as a trigger for the cyclo-reversion of the furan-maleimide cycloadduct and resulted in the shear-thinning behavior of this hydrogel (**Figure 3G**). However, after extrusion when the hydrogel was at rest and no stress was applied (**Figure 3H**), the furan and the maleimide functional groups could slowly react resulting in the observed self-healing (**Figure 3I**). Notably, the near-identical initial rate of gelation for the original and the extruded hydrogels further indicate towards force-induced cyclo-reversion of the furan-maleimide cycloadduct, as similar rate of gelation could not have been otherwise explained by considering a reaction between unreacted furan and maleimide groups from the first-time reaction during hydrogel formation.

The cycloaddition reaction between furan and maleimide can yield kinetically controlled *endo* and thermodynamically controlled *exo* adduct. The cyclo-reversion at higher temperature can also be explained considering the forward reaction (cycloaddition) being entropically unfavorable. In case of hydrogels prepared using this reaction, high temperatures and relatively long incubation times were needed to obtain self-healing from a single incision.³⁷ To our understanding, this is indicative of the thermodynamically controlled furan-maleimide cycloaddition resulting in the observed temperature triggered self-healing behavior.

Cyclo-reversion of furan-maleimide cycloadduct under mechanical force has so far been only observed in case of single polymer chains.⁵⁶⁻⁵⁸ The mechanical stretching was provided using ultrasound. Proximal cycloadducts, such as we have in the system, had been demonstrated to

undergo cyclo-reversion under mechanical stretching.⁵⁶ In a recent study, researchers have demonstrated that such cyclo-reversion under tension may follow a pericyclic or a non-pericyclic pathway depending on the amount of applied force.⁵⁵ Nonetheless, such cyclo-reversion induced by shear-stress has not been observed so far in ECM-polymer derived hydrogel. Plausible chemical structures involved in this process are depicted in **Figure 3J**. Although, it appears to be intuitive that having mechanophores within crosslinks will result in a hydrogel to be self-healing, this is vastly oversimplification. Several studies in this field debate and discuss the difficulties in activating a mechanophore in a crosslinked hydrogel system where the applied macroscopic stress was never distributed homogeneously over the complete crosslinked network and then funneled to the mechanophores.⁵⁹ In fact, only a tiny fraction of the mechanophores are usually activated through applied macroscopic stress. To our surprise, the shear-thinning and autonomous self-healing behaviors of the hydrogels developed here indicate towards mechanophore activation using macroscopic stress. To the best of our knowledge this is the only example of hydrogel of this kind. Although intriguing, it should be noted that rheology is a macroscopic evaluation technique, and apparent complete macroscopic autonomous healing in terms of rate of gelation, moduli, or linear viscoelastic limit does not necessarily imply complete healing at a nanoscale. More studies, especially those which can reveal nanoscale structural information under stress, could be great tools to explore this further which would be instrumental in rationally designing such hydrogel systems. Nevertheless, ECM-derived injectable hydrogels with shear-thinning and autonomous self-healing, shape-fidelity, and non-swelling over long term is a major leap forward in the field of injectable biomaterials.

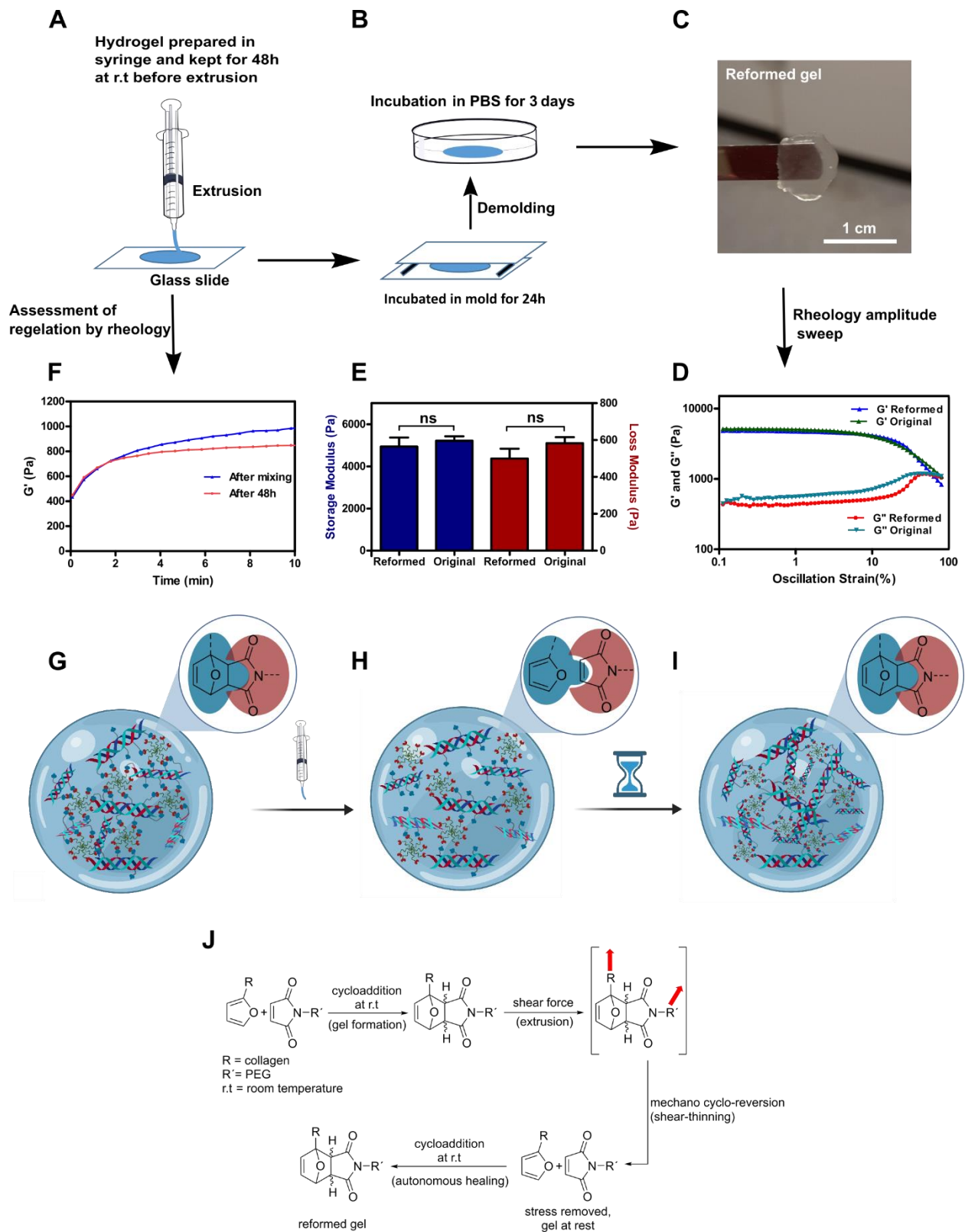


Figure 3. Autonomous self-healing properties of collagen furan hydrogels. **A-B.** Schematic of the self-healing experiment. **C.** Photograph of the reformed hydrogel. **D.** Representative dynamic oscillatory amplitude sweep of reformed hydrogels compared with original hydrogels that were kept in the mold for 3 days, followed by incubation in PBS for 3 days. **E.** The storage and loss moduli at 1 % strain of reformed hydrogels compared to original samples ($F_{389.3, df_{15}}$). **F.** Assessment of gelation by rheology time sweep at immediately after mixing of precursors and at extrusion after 48h incubation in syringe as depicted in **A**. **G-I.** Schematic representation of shear-stress induced cyclo-reversion during injection followed by cycloaddition after the stress being removed leading to shear-thinning and autonomous self-healing, respectively. **J.** Chemical structures of plausible intermediates formed during shear-thinning and autonomous self-healing (red arrows indicate stress). All experiments were performed with **r2** hydrogels. Error bars represent standard deviation, "ns" represents non-significant; df represents degrees of freedom; one-way ANOVA, followed by Tukey's test, $n = 3$ independent samples.

***In vitro* biological characterization of hydrogels.** To investigate the impact of crosslinking chemistry on cell viability, we conducted an *in vitro* assessment of cytocompatibility for **r2** hydrogels. Human fetal cardiac mesenchymal stromal cells (hfcMSCs) and Human Umbilical Vein Endothelial Cell line (HUVECs) were employed as model cells, encapsulated within these hydrogels. We evaluated cell viability at both 1 day and extended it to 7 days post-encapsulation using the Calcein-AM/ethidium homodimer Live/Dead assay, examining the fate of both hfcMSCs (**Figure 4 A-C**) and HUVECs (**Figure 4 G-I**).

Our findings reveal that cell viability consistently exceeded 80% for the developed hydrogels even up to 7 days post-cell encapsulation. This robust viability suggests that the engineered collagen furan hydrogels exhibited no cytotoxicity towards either hfcMSCs or

HUVECs. These results align with prior studies demonstrating that the Diels-Alder reaction, even during crosslinking, occurs under mild conditions and does not exert any toxicity on cells. Combined with their shear-thinning and self-healing properties, these results demonstrated the capacity of developed collagen furan hydrogels to act as a cargo for cell delivery. Moreover, cell morphology (adhesion and spreading) was assessed by fixing the cell-laden hydrogels (hfcMSCs) and staining the actin cytoskeleton with fluorescent phalloidin and nuclei with DAPI. Cell spreading in collagen furan hydrogels was evaluated by measuring the cell area under a microscope. As shown in **Figure 4D**, hfcMSCs adhered effectively to the three-dimensional hydrogel structure even one day after encapsulation. After 7 days, we observed a noticeable increase in cell adhesion and localized remodeling of the hydrogel, as evidenced by the hfcMSCs significantly spreading into the surrounding material (**Figure D, E**). Consequently, the quantified data in **Figure 4F** substantiates that the cell area had significantly increased.

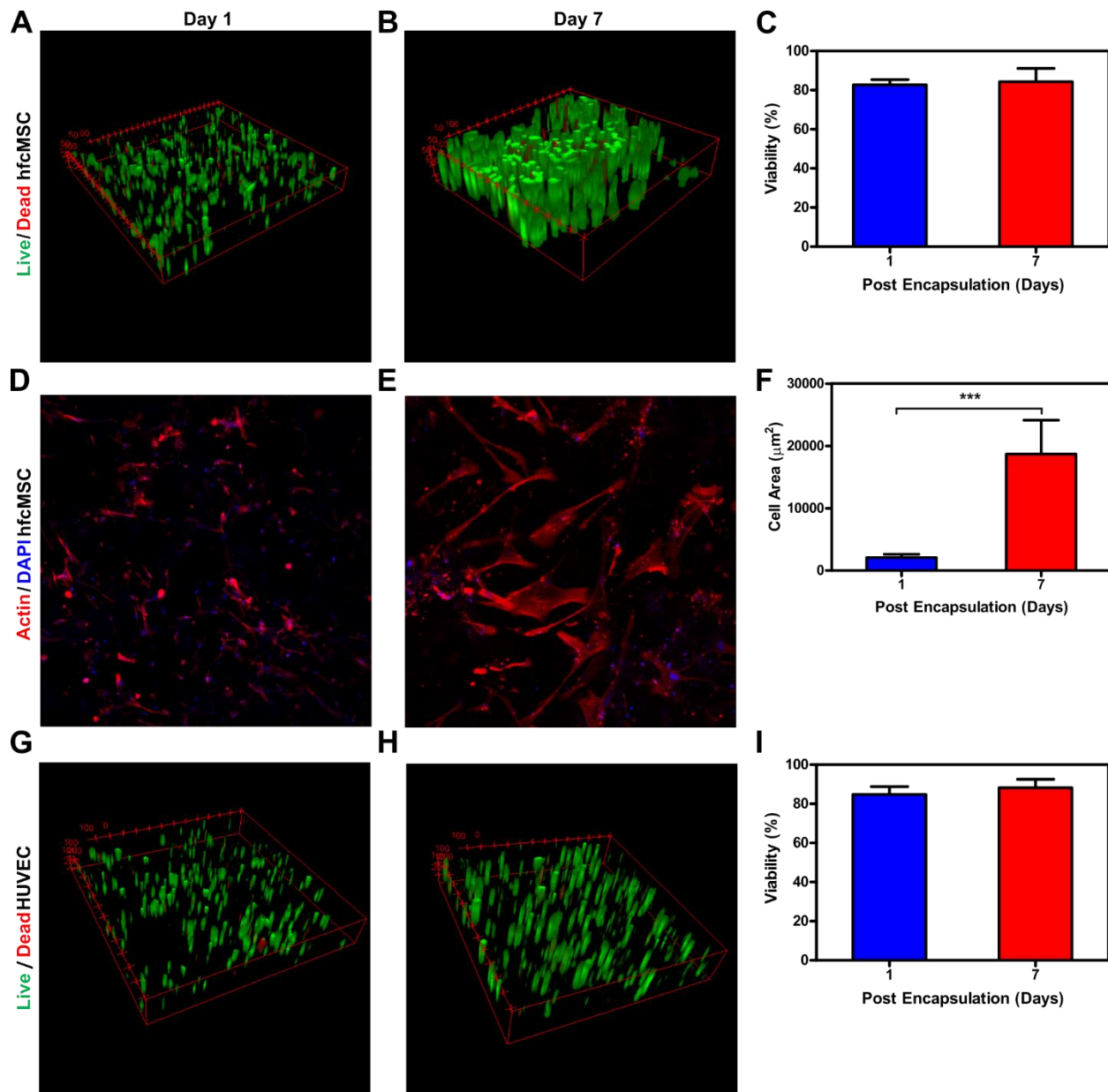


Figure 4. *In vitro* 3D cultures of hfcMSCs and HUVECs encapsulated in collagen furan hydrogels. **A.** Representative live/dead 3D scans of hfcMSCs 1 day and **B.** 7 days post encapsulation. **C.** Percentage of alive hfcMSCs for up to 7 days in 3D culture with quantification of viability images. **D.** Representative phalloidin (red)/DAPI (blue) stained images of hfcMSCs 1 day and **E.** 7 days post encapsulation. **F.** Quantification of hfcMSCs area encapsulated in hydrogels after 1 and 7 days ($F_{108.9, df_{26}}$). **G.** Representative 3D scans of HUVECs, using live/dead assay 1

day and **H.** 7 days post encapsulation. **I.** Percentage of alive HUVECs for up to 7 days in 3D culture quantification of viability images. All experiments were performed with **r2** hydrogels. Error bars represent standard deviation, "****" represents a p-value of ≤ 0.001 ; df represents degrees of freedom; one-way ANOVA, followed by Tukey's test, n = 3 independent samples.

Biocompatibility and biodegradation of the hydrogels *in vivo*. To assess the suitability of collagen-furan hydrogels for tissue engineering applications, *in vivo* biodegradation and biocompatibility were investigated using a rat subcutaneous implantation model. Cylindrical hydrogel samples (7 mm in diameter and 2 mm in height) were prepared using formulation **r2**, lyophilized, and their weights were recorded. These dried samples were subsequently implanted subcutaneously into the dorsum of male Wistar rats. A total of six rats were involved in the study, with two rats per time point, and two samples per rat. After 5, 28, and 56 days post-implantation, the rats were euthanized using CO₂ inhalation, and the samples were extracted for analysis of biodegradation and histopathology.

The explants were cleansed with PBS and deionized water, lyophilized, weighed, and subjected to direct visual inspection. Histological staining was performed on the adjacent tissue. Visual examination of the explanted samples revealed evidence of blood penetration and clotting, as indicated by a change in color to red. Additionally, the physical size of the samples decreased from day 5 to day 28, ultimately leading to complete resorption by day 56 (**Figure 5A**). As depicted in **Figure 5B**, the average dry weight of the explants showed a significant increase from 4.3 ± 1.0 mg to 6.85 ± 1.7 mg after 5 days of implantation, likely attributable to blood penetration and clotting. Subsequently, their weight decreased significantly to 3.5 ± 0.6 mg at day 28, indicative of *in vivo* biodegradation, ultimately resulting in complete resorption by day 56 post-implantation.

Furthermore, the biocompatibility of collagen-furan samples was assessed via histological analysis of subcutaneously implanted samples (**Figure 5C**). Hematoxylin and eosin (H&E) staining revealed slight to mild accumulation of lymphocytes in the adjacent tissues of samples at day 5, moderate inflammation at day 28, and rare scattered lymphocytes at day 56 post-implantation. However, no other inflammatory factors, such as giant cells or macrophages, were observed at any time point. Staining also indicated that the mean rate of fibrosis was mild at day 5, with no apparent signs of fibrous tissue formation at day 28 and day 56. The mean rate of edema was mild at day 5 and completely disappeared at day 28 and 56. Notably, granulation tissue was absent at all time points, and congestion was only observed at day 5. Integration between the samples and their adjacent tissues was visually apparent in all rats at all time points and further confirmed by staining at day 5 (**Figure S5**).

In summary, the results suggest that collagen furan hydrogels exhibit high *in vivo* biocompatibility, as evidenced by the absence of sustained inflammatory responses in the host organism. These findings collectively support the potential use of collagen furan hydrogels in biomedical applications, owing to their excellent biocompatibility and biodegradation characteristics.

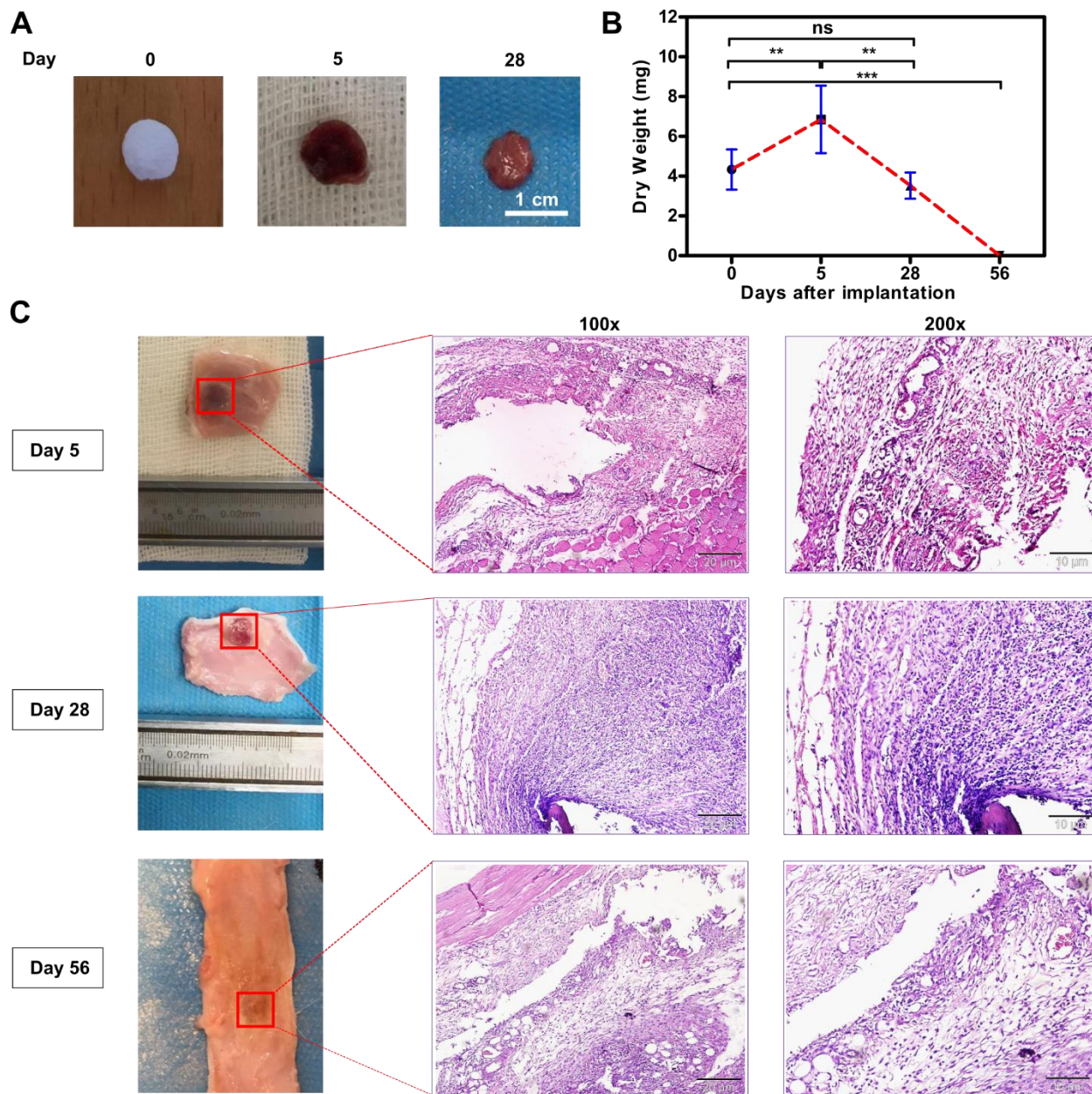


Figure 5. *In vivo* biocompatibility and biodegradation of collagen furan hydrogels using a rat subcutaneous implantation model. **A.** Representative images of collagen furan scaffold before implantation (day 0) and on days 5 and 28 post-implantation. **B.** *In vivo* biodegradation of collagen furan scaffolds on days 0, 5, 28, and 56 post-implantations ($F_{30.9}, df_{23}$). **C.** Hydrogels with the surrounding tissue after 5, 28, and 56 days of implantation and hematoxylin and eosin (H&E) staining of tissue sections (100X and 200X with scale bars 20 μ m and 10 μ m). All experiments were

performed with **r2** hydrogels. Error bars represent standard deviation, "***" represents a p-value of ≤ 0.01 , "****" represents a p-value of ≤ 0.001 , "ns" represents non-significant; df represents degrees of freedom; one-way ANOVA, followed by Tukey's test, n = 3 independent samples.

DISCUSSION

Herein we developed a collagen-based injectable hydrogel crosslinked using bio-orthogonal cycloaddition reaction between furan and maleimide. The furan-collagen developed here has similar thermal gelling properties as that of pristine collagen but is more stable upon storage compared to previously developed thiol-collagens developed for similar purposes. The resulting crosslinked hydrogel is shear-thinning, does not swell or shrink and can retain its shape and size even after prolonged storage in buffer, can be degraded by enzymes *in vitro*, and is completely resorbable *in vivo*. The developed hydrogels can be injected in a gel state and retain their injectability and shear-thinning properties up to 48 hours after mixing of the hydrogel components. This is a significant leap forward in the field of *in vivo* injectable ECM-polymer derived hydrogels since the hydrogel can be prepared in a sterile environment outside of the operation theatre and then brought to surgical room at a relevant time-point. Moreover, the injected hydrogel is capable of quantitative autonomous self-healing after injection. The existing literature on self-healing hydrogels primarily focuses on the recovery of hydrogels in terms of moduli (stiffness) after a shear-stress is applied, and very little endeavors are dedicated to assess the recovery of other crucial viscoelastic parameters such as linear viscoelastic limit, yield strength, stored and dissipated energy at varying strains, or kinetics of regelation. Moreover, in most reported cases the shear-stress from an injection is simulated by applying a single incision where the spread of the damaged zone in the hydrogel is quite limited. In contrast, a hydrogel experiences significantly higher strain and shear-rate over the whole sample during injection through a needle. The

developed hydrogel can quantitatively recover, without requiring any external trigger, from such an injection shear-stress not only in terms of moduli, but also regarding the linear viscoelastic limit and thereby, yield strength, and stored and dissipated energy at varying strains. To our surprise, even the kinetics of regelation (crosslinking) turned out to be the same as that of gelation of virgin (non-injected) sample. The observed shear-thinning and autonomous self-healing behaviors were explained by the stress-induced cyclo-reversion of the cycloadduct crosslinks followed by cycloaddition between the reacting partners to reform the gel after injection. This is the first example of an injectable collagen hydrogel which can undergo a complete autonomous self-healing after injection in terms of several viscoelastic parameters. Due to the challenges involved in mechanophore activation within a crosslinked polymer network by applying a macroscopic stress, supramolecular interactions or reversible crosslinking reactions are often thought to be better choices for designing self-healing hydrogels. However, such hydrogel systems suffer from the risk of swelling in buffer or require external trigger to favor the reverse reaction during the self-healing process. Furthermore, *in vitro* and *in vivo* experiments with cells and animal models further demonstrate the usability of the developed collagen furan hydrogels in regenerative medicine. To our knowledge, this is the first example of an injectable, shape-holding collagen hydrogel which undergo complete autonomous self-healing, where cell encapsulation is possible. The potential application of such materials could be in cardiac tissue-bulking coupled with the sustained release of encapsulated drugs where shear-stress from cardiac-beating would facilitate the release of the encapsulated drug but autonomous self-healing would recover the strength of the material and hence, the mechanical reinforcement of the ventricular wall will not be compromised during the drug release.

MATERIALS AND METHODS

Furfuryl glycidyl ether (FGE), 2,4,6-trinitrobenzenesulfonic acid (TNBS), phosphate buffered saline (PBS) powder, Trizma[®] base powder and collagenase from *Clostridium histolyticum* were purchased from Merck (Sweden). 8-arm PEG-maleimide (10 kDa) was purchased from Creative PEGWorks (USA). Porcine type I collagen (NMP collagen PS) was purchased from Nordic Biolabs (Sweden). Human Umbilical Vein Endothelial Cell line (HUVEC) was purchased from Thermo Fischer (Sweden). Human fetal cardiac mesenchymal stromal cells (hfcMSC) were obtained from Prof. Karl-Henrik Grinnemo. LIVE/DEAD[®] viability/cytotoxicity kit and Alexa Fluor[™] 594 Phalloidin were purchased from Invitrogen, Thermo Fisher (Sweden). 4,6-diamidino-2-phenylindole (DAPI) was purchased from Merck (Sweden).

Synthesis and characterization of collagen furan. Porcine type I collagen (molecular weight 300 kDa)²⁴ was dissolved in water (0.5% w/v) and deoxygenated by bubbling argon through the solution. The pH was adjusted to 10 using NaOH (2 M). After cooling the reaction mixture in an ice bath, furfuryl glycidyl ether (FGE) (three molar equivalents with respect to lysine and arginine amines considering 114 amines from lysine and arginine combined per collagen molecule) was added dropwise while stirring and maintaining the pH at 10 by intermittent addition of NaOH (2 M). The reaction mixture was left for stirring at room temperature overnight in dark under argon atmosphere. The reaction mixture was then purified by dialysis using 12-14 kDa cutoff dialysis tubes (Spectrum Laboratories, Inc., CA, USA) against deionized water with pH 10 for two days and then against deionized water with pH 4.5 for another two days. The purified collagen furan solution was lyophilized to obtain an off-white fluffy solid which was kept at -20 °C under argon until further use.

Nuclear magnetic resonance. The ^1H NMR spectroscopy was used to confirm functionalization of collagen with FGE. Proton NMR spectra of collagen furan solution in D_2O (1% (w/v)) was recorded using a JEOL JNM-ECP series FT NMR spectrometer at magnetic field strength of 9.4 T, operating at 400 MHz for ^1H NMR. Experimental conditions were as follows: 400 MHz, number of scans 20000, delay 600 s, and the spectrum was recorded at 45 °C to reduce line broadening.

Tri-nitro benzene sulfonic acid (TNBS) assay. The degree of modification of collagen furan was quantified using TNBS colorimetric assay as described earlier with minor adjustments.²³ Briefly, 2 mg of dry sample was dissolved in 200 μl of deionized water, followed by mixing with 1 ml of NaHCO_3 (4% w/w) and 1 ml of TNBS solution (0.5% w/w in water) at 40 °C under mild shaking and dark condition for 4h. Afterward, 3 mL of HCl (6 M) solution was added to quench the reaction, followed by three times extraction of unreacted TNBS from the sample with diethyl ether. UV absorbance of samples was recorded at 346 nm using a Lambda 35 UV/Vis spectrophotometer (PerkinElmer, Sweden) against a blank prepared by the above procedure, except that the HCl solution was added before the addition of TNBS solution. The same procedure was used for pristine collagen samples which were used as controls. The degree of functionalization was calculated as follows:

$$\left(\frac{(Abs_{Control} - Abs_{Blank}) - (Abs_{Sample} - Abs_{Blank})}{Abs_{Control} - Abs_{Blank}} \right) \times 100\%$$

Circular dichroism. Collagen furan and pristine collagen samples were dissolved in deionized water at a concentration of 0.02 % (w/v) and monitored using a quartz cell of 0.1 cm path length in a JASCO J-1500 spectrometer (JASCO Corporation, Tokyo, Japan). Spectra were measured

from 190 to 260 nm at 25 °C and with a scan rate of 1 nm/s. The samples were corrected against a baseline obtained by measuring deionized water.

Viscoelastic behavior of collagen furan solution. Effects of temperature on the viscoelastic behaviors of 2% (w/v) collagen furan solution were studied by dynamic oscillatory temperature sweeps using a Discovery Hybrid Rheometer 2 (TA Instruments, Sollentuna, Sweden). A 20 mm stainless steel parallel plate geometry was used. The dynamic oscillatory temperature sweeps were conducted at 1 % strain and at 1 Hz oscillation frequency, and the temperature was varied from 25 °C to 50 °C at a heating rate of 0.5 °C/min. The complex viscosity and the loss tangent were plotted against temperature.

Preparation and characterization of hydrogel. Stock solution (10% w/w) of collagen furan was prepared in deionized water and stored at 4 °C. Hydrogels were prepared by mixing collagen furan stock solution and 8-arm PEG maleimide (10 kDa) in PBS using a syringe mixing system as described previously.²⁴ The final concentration of collagen furan in the hydrogel was maintained at 2% (w/w). Four different formulations were prepared by changing the concentration of PEG maleimide in hydrogel to obtain a furan to maleimide ratio of 1:1, 1:2, 1:3, and 1:4 (**r1**, **r2**, **r3**, **r4**). Collagen-furan gel was prepared by extruding ~100 µl of the mixed components between two glass slides separated by a 1 mm spacer and cured overnight in a humid atmosphere and then stored in PBS at room temperature for 3 days before subjecting to further analyses.

Viscoelastic behavior of different hydrogel formulations. To study viscoelastic properties of different hydrogel formulations (**r1-r4**), dynamic oscillatory amplitude sweeps were performed using an 8 mm parallel plate stainless steel geometry with a constant axial load of 100 mN, at a frequency of 1 Hz and strain was swept from 0.1 to 100 %. Hydrogel discs were demolded after

curing overnight at room temperature in a humid atmosphere and then incubated in PBS for three days to reach their equilibrium swelling. Storage moduli (G'), loss moduli (G''), and loss tangent ($\tan\delta$) were calculated. All measurements were performed at 25 °C.

Compressive properties of different hydrogel formulations. Compressive properties of hydrogel formulations (**r1-r4**) were assessed using a mechanical tester (Shimadzu AGS-X universal, electromechanical) with a 10 N load cell. Samples were prepared in cylindrical molds (7 mm in diameter and 5 mm in height) and cured overnight in a humid atmosphere. Hydrogels were then demolded and incubated in PBS for 24 h prior to testing. A digital caliper was used to measure the dimensions of each hydrogel. Hydrogels were then compressed at a head speed of 1 mm/min until sample failure. The compressive modulus was determined by obtaining the slope of the linear region (0.01 – 0.1 mm/mm strain) of the stress (kPa) versus strain (mm/mm) curve.

Assessment of gelation. Dynamic oscillatory time sweep was conducted at a frequency of 1 Hz and oscillation strain of 1 % with constant axial load of 100 mN using a 20 mm stainless steel parallel plate geometry at 25 and 37 °C. Approximately 500 μ L of **r2** hydrogel were extruded onto the rheometer plate immediately after mixing of the components. Drying of the hydrogel samples was minimized by using a rheometer solvent trap. Since the storage modulus could not reach plateau until 44 hours, a longer experiment was needed. However, sample drying turned out to be an issue even when the rheometer solvent trap was used for experiments longer than 44 hours. Hence, **r2** hydrogel samples were cast and cured in the mold under humid atmosphere for 1, 3, and 7 days at room temperature and measured at each time point by a rheological amplitude sweep at 1 Hz oscillation frequency while varying the strain from 0.1 to 100 % at room temperature. The storage moduli at 1 % strain, which is within the linear region for all samples, was compared to find out the time required for complete gelation.

Shear-thinning. To evaluate the shear-thinning properties of **r2** hydrogels, viscosity was measured with increasing shear rate from 0.01 to 100 s⁻¹ in a continuous flow measurement under a constant axial load of 100 mN using a 20 mm stainless steel parallel plate geometry. Approximately 500 μL of **r2** hydrogels were extruded onto the rheometer plate immediately, 4h, and 48h after mixing of the components. Measurements were performed at 25 °C.

Enzymatic degradation. To evaluate enzymatic degradation *in vitro*, **r2** hydrogel was incubated for 1 h in Tris-HCl buffer (pH 7.4) at 37 °C. They were then placed in a vial containing preheated 5 U/mL collagenase solution in 0.1M Tris-HCL (pH 7.4) and 5mM CaCl₂ and incubated at 37 °C. At indicated time points, hydrogels were weighed after blotting excess liquid using a filter paper and percentage of hydrogel mass remaining (M_t) relative to the original swollen mass M_0 was calculated ($\frac{M_t - M_0}{M_0}$). Fresh preheated collagenase solution was replaced for each sample at each time point.

Swelling of hydrogel. To characterize the swelling, **r2** hydrogels were cut into 8 mm diameter discs, blotted with filter paper and their initial weights were recorded (M_0). The samples were then incubated in 1 mL of PBS buffer at 37 °C for indicated duration. At selected time intervals, the excess liquid was removed from the swollen gels and the samples were reweighed (M_t). Hydrogels were then replenished with fresh buffer. From these data, swelling ratios ($\frac{M_t - M_0}{M_0}$) were calculated, and the equilibrium swelling ratio was recorded when the mass of the hydrogels no longer increased.

Self-healing properties of hydrogel. To evaluate self-healing properties of **r2** hydrogels after extrusion, hydrogel precursor components were first mixed in a syringe mixing system and kept

for curing in the syringe for 48 h at room temperature. Afterwards, the crosslinked hydrogel in the syringe was extruded and cast between two glass slides that were separated by a 1 mm spacer and cured overnight in a humid atmosphere and then stored in PBS for 3 days at room temperature. To study viscoelastic properties of reformed hydrogels, dynamic oscillatory amplitude sweep was performed using an 8 mm parallel plate stainless steel geometry under a constant axial load of 100 mN, at 1 Hz and compared with **r2** hydrogels that were extruded immediately from the syringe mixing system after mixing of the components, kept in the mold for 3 days, followed by incubation in PBS for 3 days before subjecting to rheological amplitude sweep.

The gelation of **r2** hydrogels after extrusion was compared with non-extruded sample. For this purpose, hydrogel precursor components were mixed in a syringe mixing system, kept for curing in the syringe for 48 h at room temperature, and then extruded directly onto the rheometer plate. A dynamic oscillatory time sweep was conducted at 1 Hz oscillation frequency, 1 % oscillation strain, and 25 °C with constant axial load of 100 mN using a 20 mm stainless steel parallel plate geometry and compared with hydrogel that was extruded onto the rheometer plate directly after mixing of the components.

***In vitro* biocompatibility studies**

Cell culture. Human fetal cardiac mesenchymal stromal cells (hfcMSC) and human umbilical vein endothelial cells (HUVEC; ATCC) were used for *in vitro* studies. hfcMSCs were cultured using MSC growth medium (MSC-GM, Lonza), supplemented with fetal bovine serum (10%) and penicillin - streptomycin (1%). HUVECs were maintained in endothelial basal medium (EBM-2, Lonza) enriched with endothelial growth factors (BulletKit, Lonza) and 100 units/ml penicillin-streptomycin (Gibco, USA). All cell cultures were maintained in the cell culture incubator (37 °C,

5% CO₂). Cells were passaged approximately 2 times per week and media was changed every second day.

Cell encapsulation. Collagen furan hydrogels (**r2**) were prepared according to the same protocol mentioned above, except for using cell media instead of PBS. Cells were trypsinized and resuspended in a minimal amount of cell growth medium. For encapsulation experiments, cells (either hfcMSC or HUVEC) were mixed into the hydrogel by gentle pipetting to yield the final cell concentration in the hydrogel of 200,000 cells/200 μ L and 300,000 cells/200 μ L, respectively, and transferred into a syringe. Cell-laden hydrogels were cast into 48 well plates and cured for 1 h at 37 °C in cell culture incubator, followed by adding the appropriate cell growth medium. Media was changed every 2 days.

Cell viability. A commercial LIVE/DEAD Viability/Cytotoxicity Kit (Invitrogen, Thermo Fisher, Sweden) was used to evaluate cell viability according to instructions from the manufacturer. Cell viability was evaluated after 1 and 7 days of culture. Briefly, culture medium was aspirated and the hydrogels were washed with 1X sterile PBS and then incubated with 0.5 μ L/ mL of calcein AM and 2 μ L/mL of ethidium homodimer in PBS for 45 min in dark at 37 °C. Live cells were stained green, whereas dead cells were stained red. The cell-carrying hydrogels were imaged with a Zeiss LSM700 confocal microscope (Germany) and 3-D stacking and Z-sectioning was performed using LSM700 software. For each sample, at least five independent z-stacks at 10x magnification were analyzed. Cell viability was calculated as the ratio of live cells to the total number of cells using ImageJ software (n = 3).

Cell adhesion, morphology, and spreading. Fluorescent staining of F-actin filaments with Alexa Fluor 594TM phalloidin (Invitrogen) and cell nuclei with 4,6-diamidino-2-phenylindole (DAPI; Sigma) was used to investigate attachment and spreading of encapsulated cells inside hydrogels.

To stain F-actin filaments of the cell, cell-laden hydrogels were fixed in 4% (v/v) paraformaldehyde (Sigma) for 30 min at room temperature and washed with PBS. The cells were then permeabilized in a 0.1% (w/v) Triton X-100 solution in PBS for 20 min and blocked in 1% (w/v) bovine serum albumin (BSA) for 1 h. The samples were then incubated in a solution of 1:40 ratio of Alexa Fluor 594™ phalloidin in 0.1% BSA for 45 min at room temperature to stain the actin cytoskeleton. For DAPI staining, the cell-laden hydrogels were incubated in a 0.1% (v/v) DAPI solution in PBS for 10 min at 37 °C to stain the nuclei. The stained samples were then washed three times with PBS before visualizing with a Zeiss LSM700 confocal microscope (Germany).

***In vivo* biodegradation and biocompatibility**

Dorsal subcutaneous implantation of hydrogels. All animal protocols were approved by the Institutional Animal Care and Use Committee (IR.MUI.REC.1402.022) at Isfahan University. Male Wistar rats (200 - 250 g) were purchased from Dental Research Center (Prof. Torabi Nejad Dentistry Research Center, Isfahan School of Dentistry, Isfahan, Iran) and kept in the animal core facility at Isfahan University (Water and Electrolyte Research Center, Isfahan University of Medical Sciences, Isfahan, Iran). Hydrogels were prepared under sterile conditions in cylindrical molds as described for compression testing and their initial dry weights (day 0) were recorded after air drying. General anesthesia and analgesia were induced by intra-peritoneal injection of 50 mg/kg ketamine and 5 mg/kg xylazine. Two 1 cm incisions were created on the posterior dorsomedial skin of the animals, and lateral subcutaneous pockets were prepared by blunt dissection. Dry hydrogels were then implanted into the subcutaneous pockets, followed by suture and recovery from anesthesia.

***In vivo* degradation and histopathological analysis.** On days 5, 28, and 56 post implantations, the animals were euthanized by CO₂ inhalation, and the samples were explanted for biodegradation and histopathological analysis. For biodegradation studies, the samples were carefully cleaned to remove the adjacent tissue and then washed three times with PBS and deionized water. Samples were then lyophilized to measure the weight loss over time.

For histological analysis, the surrounding tissues were fixed in 10% (v/v) formalin overnight. After fixation, the tissues were washed in running tap water for 24 h. Afterward, it was dehydrated in graded alcohols, cleared in xylene, and embedded in paraffin. 4 µm sections were taken from paraffin blocks with the help of a Leica RM2145 microtome. The slides were then stained for hematoxylin and eosin (H&E) staining (Sigma) according to the manufacturer's instructions. The examinations were carried out under the Olympus U-TV0.63XC microscope (Japan).

Statistical analyses. All experiments were performed at least in triplicate, and data are presented as mean ± standard deviation (SD). Statistical analysis was performed in GraphPad Prism software. One-way ANOVA tests were performed to determine statistical significance, and p values less than 0.05 were considered as significant.

Author contributions

A.S. conceived the project, M.J., A.S., S.S., and A.T. designed the experiments. M.J. and S.S. performed the experiments and analyzed the data. M.J. and A.S. wrote the paper with input from all authors.

Corresponding author. *Email: ayan.samanta@kemi.uu.se

Acknowledgments

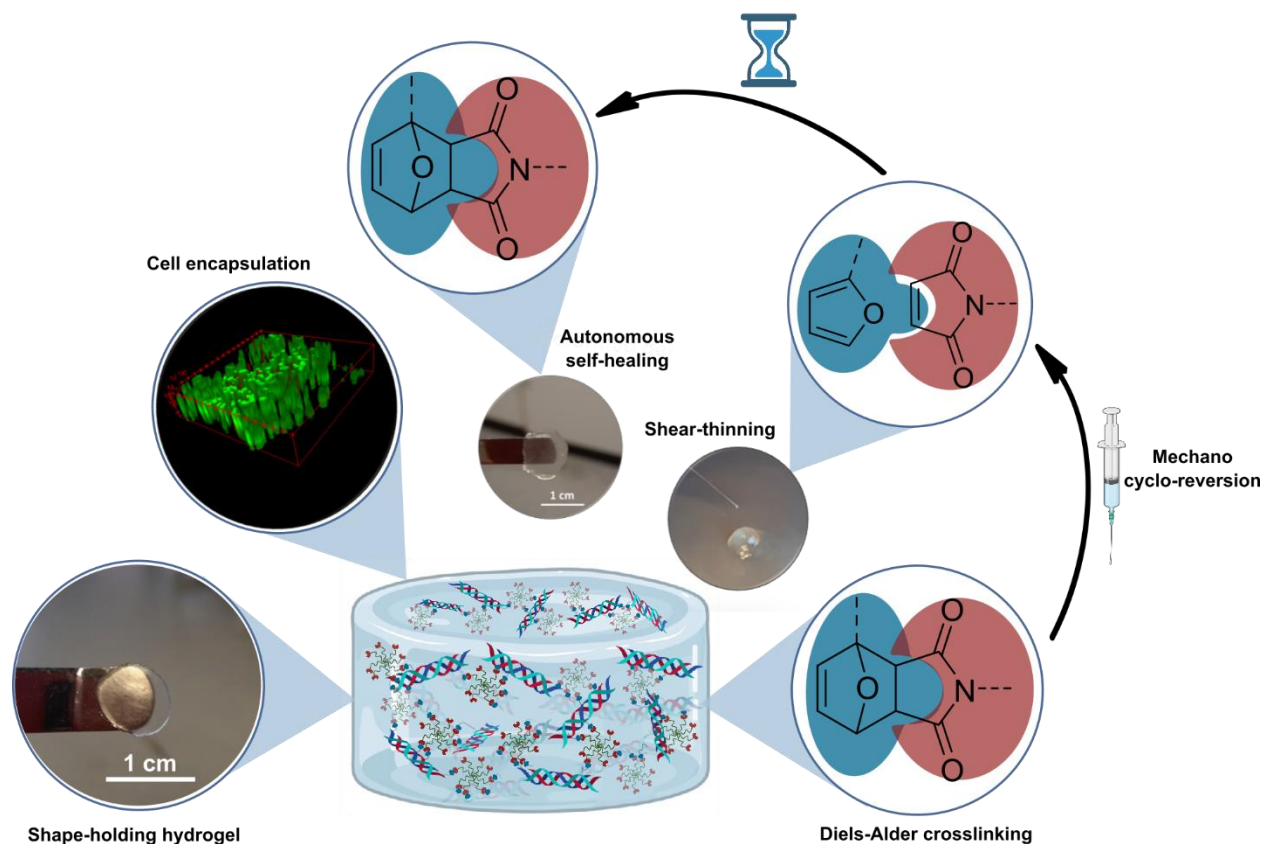
This work was funded by Olle Engvist (189-0263), Lars Hiertas Minne (FO2018-0479), Stiftelsen Promobilia (20056), Strategiska Forskningsområden (2009-1035), and institutional support from Macromolecular Chemistry Research Program. Authors thank Professor Karl-Henrik Grinnemo for providing hfcMSCs and Professor Debashree Ghosh for fruitful advice on DFT calculations.

Additional information

Electronic Supplementary Information accompanies this paper at <https://.....>

Competing interests: The authors declare no competing financial interests.

Table Of Content (TOC) Graphic



REFERENCES

1. Raucci, M.G., D'Amora, U., Ronca, A. & Ambrosio, L. Injectable functional biomaterials for minimally invasive surgery. *Advanced Healthcare Materials* **9**, 2000349 (2020).
2. Capuani, S., Malgir, G., Chua, C.Y.X. & Grattoni, A. Advanced strategies to thwart foreign body response to implantable devices. *Bioeng Transl Med* **7** (2022).
3. Paez, J.I., Farrukh, A., Valbuena-Mendoza, R., Wlodarczyk-Biegun, M.K. & del Campo, A. Thiol-Methylsulfone-Based Hydrogels for 3D Cell Encapsulation. *Acs Applied Materials & Interfaces* **12**, 8062-8072 (2020).
4. Dimatteo, R., Darling, N.J. & Segura, T. In situ forming injectable hydrogels for drug delivery and wound repair. *Advanced drug delivery reviews* **127**, 167-184 (2018).
5. Uman, S., Dhand, A. & Burdick, J.A. Recent advances in shear-thinning and self-healing hydrogels for biomedical applications. *Journal of Applied Polymer Science* **137** (2020).
6. Feng, W. & Wang, Z. Tailoring the Swelling-Shrinkable Behavior of Hydrogels for Biomedical Applications. *Adv Sci* **10**, 2303326 (2023).
7. Lam, N.T., Lam, H., Sturdivant, N.M. & Balachandran, K. Fabrication of a matrigel-collagen semi-interpenetrating scaffold for use in dynamic valve interstitial cell culture. *Biomed Mater* **12** (2017).
8. Griffith, M., Samanta, A. & Jangamreddy, J.R. (U.S. Patent No. 11,426,492. 30 Aug. 2022).
9. Nazir, R., Bruyneel, A., Carr, C. & Czernuszka, J. Collagen type I and hyaluronic acid based hybrid scaffolds for heart valve tissue engineering. *Biopolymers*, e23278 (2019).
10. Bax, D.V. et al. Fundamental insight into the effect of carbodiimide crosslinking on cellular recognition of collagen-based scaffolds. *Acta biomaterialia* **49**, 218-234 (2017).
11. Gao, Y. et al. Fabrication and characterization of collagen-based injectable and self-crosslinkable hydrogels for cell encapsulation. *Colloids Surf B Biointerfaces* **167**, 448-456 (2018).
12. Haagdoorens, M. et al. Plant Recombinant Human Collagen Type I Hydrogels for Corneal Regeneration. *Regen Eng Transl Med* **8**, 269-283 (2022).
13. Samarawickrama, C. et al. Collagen-Based Fillers as Alternatives to Cyanoacrylate Glue for the Sealing of Large Corneal Perforations. *Cornea* **37**, 609-616 (2018).
14. Fernandes-Cunha, G.M. et al. In situ-forming collagen hydrogel crosslinked via multi-functional PEG as a matrix therapy for corneal defects. *Sci Rep-Uk* **10** (2020).
15. Casali, D.M., Yost, M.J. & Matthews, M.A. Eliminating glutaraldehyde from crosslinked collagen films using supercritical CO. *J Biomed Mater Res A* **106**, 86-94 (2018).
16. Umashankar, P.R., Mohanan, P.V. & Kumari, T.V. Glutaraldehyde treatment elicits toxic response compared to decellularization in bovine pericardium. *Toxicol Int* **19**, 51-58 (2012).
17. Pupkaite, J. et al. Collagen-Based Photoactive Agent for Tissue Bonding. *Acs Applied Materials & Interfaces* **9**, 9265-9270 (2017).
18. Nguyen, T.U., Watkins, K.E. & Kishore, V. Photochemically crosslinked cell-laden methacrylated collagen hydrogels with high cell viability and functionality. *J Biomed Mater Res A* **107**, 1541-1550 (2019).
19. Gaudet, I.D. & Shreiber, D.I. Characterization of Methacrylated Type-I Collagen as a Dynamic, Photoactive Hydrogel. *Biointerphases* **7**, doi: 10.1007/s13758-13012-10025-y (2012).

20. Guo, K. et al. Collagen-Based Thiol-Norbornene Photoclick Bio-Ink with Excellent Bioactivity and Printability. *Acs Applied Materials & Interfaces* **13**, 7037-7050 (2021).
21. Zhang, H. et al. Penetration depth of photons in biological tissues from hyperspectral imaging in shortwave infrared in transmission and reflection geometries. *Journal of biomedical optics* **21**, 126006 (2016).
22. Pupkaite, J., Rosenquist, J., Hilborn, J. & Samanta, A. Injectable Shape-Holding Collagen Hydrogel for Cell Encapsulation and Delivery Cross-linked Using Thiol-Michael Addition Click Reaction. *Biomacromolecules* **20**, 3475-3484 (2019).
23. Ravichandran, R. et al. Functionalised type-I collagen as a hydrogel building block for bio-orthogonal tissue engineering applications. *Journal of Materials Chemistry B* **4**, 318-326 (2016).
24. Rosenquist, J. et al. An Injectable, Shape-Retaining Collagen Hydrogel Cross-linked Using Thiol-Maleimide Click Chemistry for Sealing Corneal Perforations. *ACS Appl Mater Interfaces* **15**, 34407-34418 (2023).
25. Morozova, S.M. Recent Advances in Hydrogels via Diels-Alder Crosslinking: Design and Applications. *Gels-Basel* **9** (2023).
26. Chen, F., Le, P., Fernandes-Cunha, G.M., Heilshorn, S.C. & Myung, D. Bio-orthogonally crosslinked hyaluronate-collagen hydrogel for suture-free corneal defect repair. *Biomaterials* **255**, 120176 (2020).
27. Lee, H.J., Fernandes-Cunha, G.M., Na, K.S., Hull, S.M. & Myung, D. Bio-Orthogonally Crosslinked, In Situ Forming Corneal Stromal Tissue Substitute. *Adv Healthc Mater* **7**, e1800560 (2018).
28. Koshy, S.T. et al. Click-Crosslinked Injectable Gelatin Hydrogels. *Advanced Healthcare Materials* **5**, 541-547 (2016).
29. Negrini, N.C., Volponi, A.A., Sharpe, P.T. & Celiz, A.D. Tunable Cross-Linking and Adhesion of Gelatin Hydrogels via Bioorthogonal Click Chemistry. *Acs Biomaterials Science & Engineering* **7**, 4330-4346 (2021).
30. Nimmo, C.M., Owen, S.C. & Shoichet, M.S. Diels-Alder Click Cross-Linked Hyaluronic Acid Hydrogels for Tissue Engineering. *Biomacromolecules* **12**, 824-830 (2011).
31. Baker, A.E.G., Tam, R.Y. & Shoichet, M.S. Independently Tuning the Biochemical and Mechanical Properties of 3D Hyaluronan-Based Hydrogels with Oxime and Diels-Alder Chemistry to Culture Breast Cancer Spheroids. *Biomacromolecules* **18**, 4373-4384 (2017).
32. Fisher, S.A., Anandakumaran, P.N., Owen, S.C. & Shoichet, M.S. Tuning the Microenvironment: Click-Crosslinked Hyaluronic Acid-Based Hydrogels Provide a Platform for Studying Breast Cancer Cell Invasion. *Adv Funct Mater* **25**, 7163-7172 (2015).
33. Smith, L.J. et al. Diels Alder Click-Cross-Linked Hydrogels with Increased Reactivity Enable 3D Cell Encapsulation. *Biomacromolecules* **19**, 926-935 (2018).
34. Yu, F., Cao, X.D., Zeng, L., Zhang, Q. & Chen, X.F. An interpenetrating HA/G/CS biomimic hydrogel via Diels-Alder click chemistry for cartilage tissue engineering. *Carbohydrate Polymers* **97**, 188-195 (2013).
35. Owen, S.C., Fisher, S.A., Tam, R.Y., Nimmo, C.M. & Shoichet, M.S. Hyaluronic Acid Click Hydrogels Emulate the Extracellular Matrix. *Langmuir* **29**, 7393-7400 (2013).
36. Ghanian, M.H., Mirzadeh, H. & Baharvand, H. In Situ Forming, Cytocompatible, and Self-Recoverable Tough Hydrogels Based on Dual Ionic and Click Cross-Linked Alginate. *Biomacromolecules* **19**, 1646-1662 (2018).

37. Li, D.Q. et al. Fabrication of self-healing pectin/chitosan hybrid hydrogel via Diels-Alder reactions for drug delivery with high swelling property, pH-responsiveness, and cytocompatibility. *Carbohydrate Polymers* **268** (2021).
38. Fan, M. et al. Biodegradable hyaluronic acid hydrogels to control release of dexamethasone through aqueous Diels-Alder chemistry for adipose tissue engineering. *Materials Science & Engineering C-Materials for Biological Applications* **56**, 311-317 (2015).
39. Yang, Y.L. et al. Controlled release of MSC-derived small extracellular vesicles by an injectable Diels-Alder crosslinked hyaluronic acid/PEG hydrogel for osteoarthritis improvement. *Acta Biomaterialia* **128**, 163-174 (2021).
40. Garcia-Astrain, C. et al. Diels-Alder "click" chemistry for the cross-linking of furfuryl-gelatin-polyetheramine hydrogels. *Rsc Advances* **4**, 35578-35587 (2014).
41. Magli, S. et al. Design and Synthesis of Chitosan-Gelatin Hybrid Hydrogels for 3D Printable in vitro Models. *Front Chem* **8**, 524 (2020).
42. Debone Piazza, R., Brandt, J.V., Carvalho dos Santos, C., Fernando Costa Marques, R. & Jafelicci Junior, M. Gelatin/dextran-based hydrogel cross-linked by Diels-Alder click chemistry: the swelling and potassium diclofenac releasing. *Medical Devices & Sensors* **4**, e10151 (2021).
43. Garcia-Astrain, C. et al. Biocompatible Hydrogel Nanocomposite with Covalently Embedded Silver Nanoparticles. *Biomacromolecules* **16**, 1301-1310 (2015).
44. Garcia-Astrain, C. et al. Maleimide-grafted cellulose nanocrystals as cross-linkers for bionanocomposite hydrogels. *Carbohydrate Polymers* **149**, 94-101 (2016).
45. Garcia-Astrain, C. et al. Effect of maleimide-functionalized gold nanoparticles on hybrid biohydrogels properties. *Rsc Advances* **5**, 50268-50277 (2015).
46. Garcia-Astrain, C. et al. Designing hydrogel nanocomposites using TiO₂ as clickable cross-linkers. *J Mater Sci* **51**, 5073-5081 (2016).
47. Drzewiecki, K.E., Grisham, D.R., Parmar, A.S., Nanda, V. & Shreiber, D.I. Circular Dichroism Spectroscopy of Collagen Fibrillogenesis: A New Use for an Old Technique. *Biophysical journal* **111**, 2377-2386 (2016).
48. Zhang, M., Chen, Y.H., Li, G.Y. & Du, Z.L. Rheological properties of fish skin collagen solution : Effects of temperature and concentration. *Korea-Aust Rheol J* **22**, 119-127 (2010).
49. Lai, G.L., Li, Y. & Li, G.Y. Effect of concentration and temperature on the rheological behavior of collagen solution. *Int J Biol Macromol* **42**, 285-291 (2008).
50. Egli, J., Siebler, C., Kohler, M., Zenobi, R. & Wennemers, H. Hydrophobic Moieties Bestow Fast-Folding and Hyperstability on Collagen Triple Helices. *J Am Chem Soc* **141**, 5607-5611 (2019).
51. Sakai, T. et al. Design and fabrication of a high-strength hydrogel with ideally homogeneous network structure from tetrahedron-like macromonomers. *Macromolecules* **41**, 5379-5384 (2008).
52. Oechsle, A.M., Wittmann, X., Gibis, M., Kohlus, R. & Weiss, J. Collagen entanglement influenced by the addition of acids. *European Polymer Journal* **58**, 144-156 (2014).
53. Tsenoglou, C. Rubber Elasticity of Cross-Linked Networks with Trapped Entanglements and Dangling Chains. *Macromolecules* **22**, 284-289 (1989).
54. Safaei, A., Terryn, S., Vanderborght, B., Van Assche, G. & Brancart, J. The Influence of the Furan and Maleimide Stoichiometry on the Thermoreversible Diels-Alder Network Polymerization. *Polymers* **13** (2021).

55. Cardosa-Gutierrez, M., De Bo, G., Duwez, A.S. & Remacle, F. Bond breaking of furan-maleimide adducts a diradical sequential mechanism under an external mechanical force. *Chemical Science* **14**, 1263-1271 (2023).
56. Stevenson, R. & De Bo, G. Controlling Reactivity by Geometry in Retro-Diels-Alder Reactions under Tension. *J Am Chem Soc* **139**, 16768-16771 (2017).
57. Wang, Z. & Craig, S.L. Stereochemical effects on the mechanochemical scission of furan-maleimide Diels-Alder adducts. *Chem Commun* **55**, 12263-12266 (2019).
58. Zhang, M. & De Bo, G. Impact of a Mechanical Bond on the Activation of a Mechanophore. *J Am Chem Soc* **140**, 12724-12727 (2018).
59. Brown, C.L. & Craig, S.L. Molecular engineering of mechanophore activity for stress-responsive polymeric materials. *Chemical Science* **6**, 2158-2165 (2015).

Electronic Supplementary Information for

*Shear-Induced Cyclo-Reversion Leading to Shear-Thinning and Autonomous Self-Healing
in an Injectable, Shape-Holding Collagen Hydrogel*

Mahsa Jamadi Khiabani,¹ Sareh Soroushzadeh,² Ardeshir Talebi,² and Ayan Samanta*.¹

¹Macromolecular Chemistry, Department of Chemistry – Ångström Laboratory, Uppsala University, Box 538, 751 21 Uppsala, Sweden

²Department of Pathology, School of Medicine, Isfahan University of Medical Sciences, Isfahan, Iran

*Corresponding author: ayan.samanta@kemi.uu.se

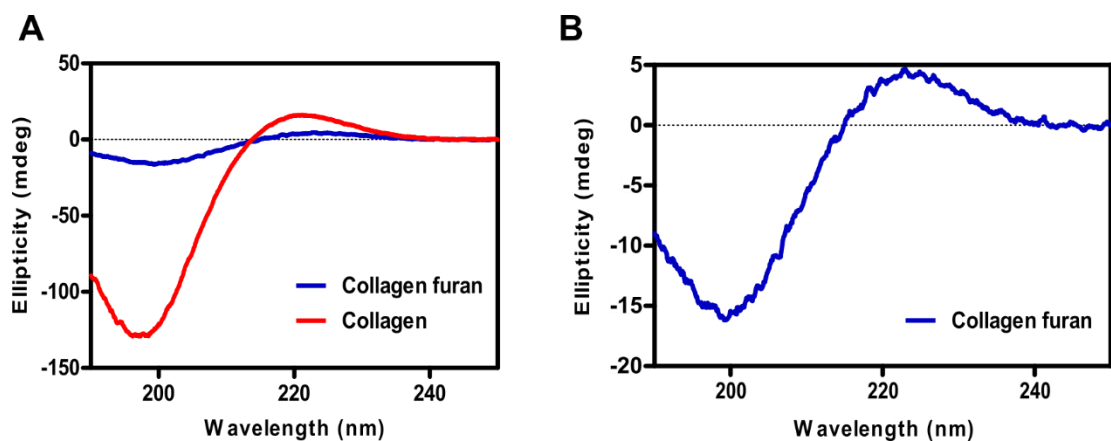


Figure S1. Circular dichroism spectra; **A:** collagen furan and pristine collagen, **B:** magnified view of collagen furan.

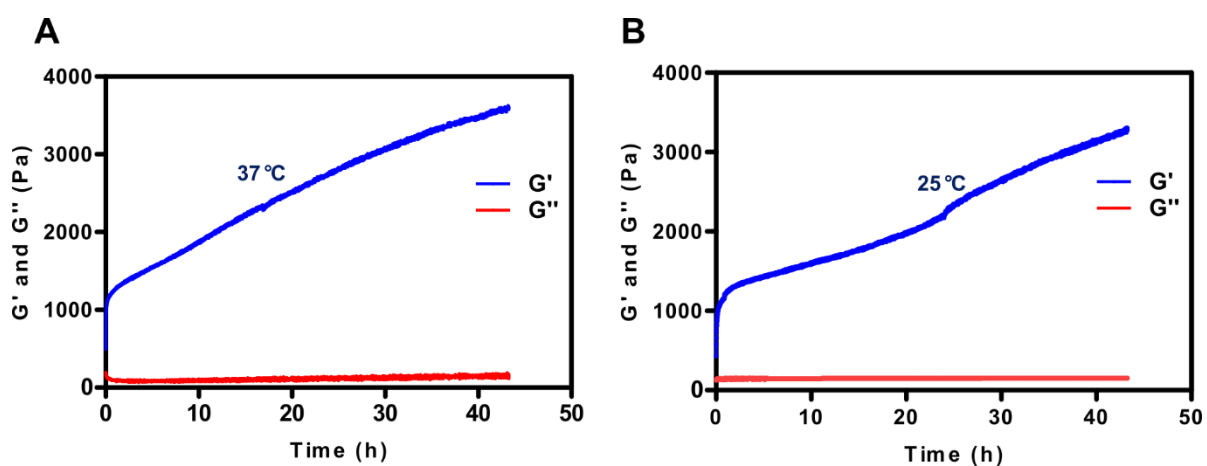


Figure S2. Dynamic oscillatory time sweep to monitor gelation; **A:** experiment conducted at 37 °C, **B:** experiment conducted at 25 °C. Formulation used **r2**.

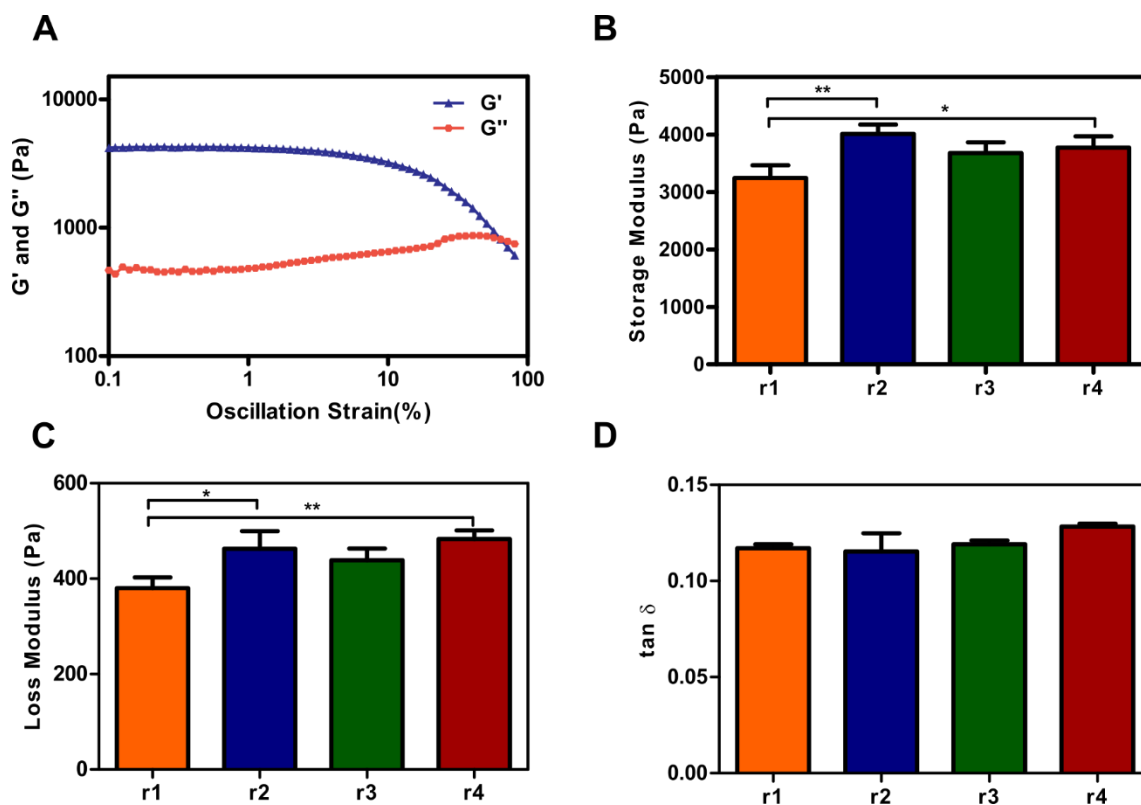


Figure S3. Characterization of the viscoelastic properties of collagen furan hydrogels (**r1 - r4**); **A:** representative dynamic oscillatory amplitude sweep of **r2** hydrogel, **B:** storage moduli of all hydrogels (**r1 - r4**) at 1 Hz oscillation frequency and 1% oscillation strain ($F_{8,279}$, df_{11}), **C:** loss moduli of all hydrogels (**r1 - r4**) at 1 Hz oscillation frequency and 1% oscillation strain ($F_{8,518}$, df_{11}), **D:** loss tangent of all hydrogels (**r1 - r4**) at 1 Hz oscillation frequency and 1% oscillation strain. All measurements were performed at 25 °C. Error bars represent standard deviation, "*" represents a p-value of ≤ 0.05 , "***" represents a p-value of ≤ 0.01 ; df represents degrees of freedom; one-way ANOVA, followed by Tukey's test, $n = 3$ independent samples.

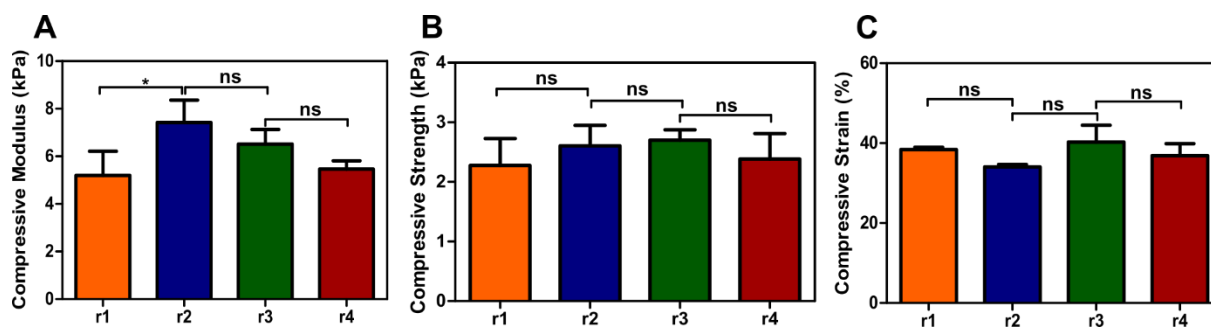


Figure S4. Unconfined compression of collagen furan hydrogels (**r1 - r4**); **A:** compressive moduli derived from the linear region (0.01 - 0.1 mm/mm strain) of the stress-strain curve ($F_{5.167, df_{11}}$), **B:** compressive strength of hydrogels at failure ($F_{0.850, df_{11}}$), **C:** compressive strain of hydrogels at failure ($F_{3.009, df_{11}}$). All measurements were performed at 25 °C. Error bars represent standard deviation, "*" represents a p-value of ≤ 0.05 , "ns" represents nonsignificant; df represents degrees of freedom; one-way ANOVA, followed by Tukey's test, $n = 3$ independent samples.

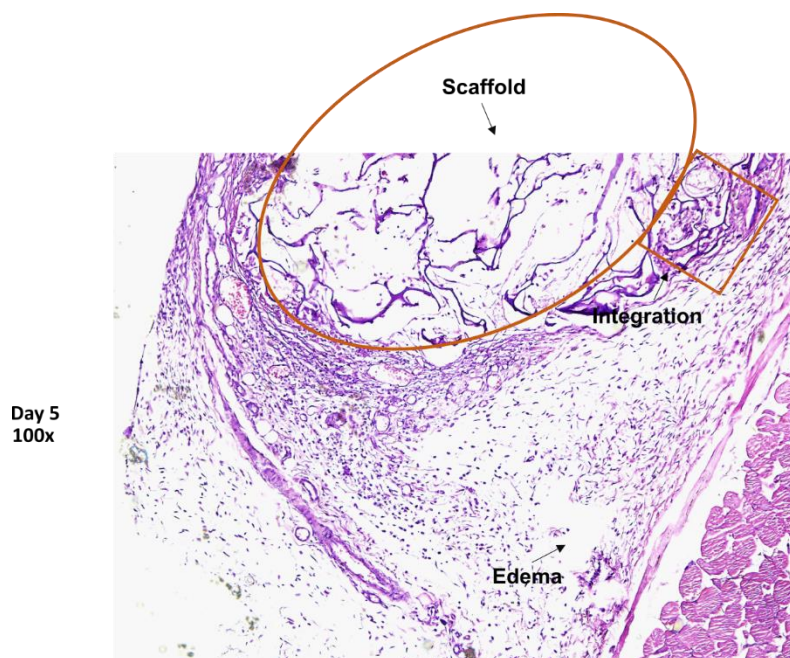


Figure S5. Hematoxylin and eosin (H&E) staining of collagen furan hydrogel (**r2**) with the surrounding tissue after 5 days of implantation, showing the integration and ingrowth of noninflammatory tissue into the scaffold.

Table S1. Different collagen furan hydrogel formulations used in this study.

Name	Formulation Furan to maleimide	Collagen concentration		PEG concentration		Furan concentration	Maleimide concentration
		[%]	[μ M]	[%]	[μ M]	[μ M]	[μ M]
r1	1:1	2	67	0.58	580	4659	4640
r2	1:2	2	67	1.16	1160	4659	9280
r3	1:3	2	67	1.74	1740	4659	13920
r4	1:4	2	67	2.32	2320	4659	18560